Supplemental Information

Rational design of flower-like Co-Zn LDH@$Co(H_2PO_4)_2$ heterojunction as advanced electrode material for supercapacitors

Miao He[a], Yi He[c], Xinyi Zhou[a], Qiang Hu[a], Shixiang Ding[a], Qiaoji Zheng[a], Dunmin Lin[a,*], Xijun Wei[b,*]

[a]College of Chemistry and Materials Science, Sichuan Normal University, Chengdu 610066, China

[b]State Key Laboratory of Environment-Friendly Energy Materials, School of Materials Science and Engineering, Southwest University of Science and Technology, Mianyang, 621010, P. R. China.

[c]Ecology and Health Institute, Hangzhou Vocational & Technical College, Hangzhou 310018, China

[*] Corresponding author: Email: ddmd222@sicnu.edu.cn (Dunmin Lin); xijunwei1992@swust.edu.cn (Xijun Wei); Fax: +86 28 84760802 Tel: +86 28 84760802

1. Experimental Section

1.1. Chemicals

All chemical reagents were analytical and used directly without any further purification. The raw materials were as follows: Zinc(Ⅱ) nitrate hexahydrate ($Zn(NO)_3 \cdot 6H_2O$), Cobaltous(Ⅱ) Nitrate Hexahydrate ($Co(NO)_3 \cdot 6H_2O$), urea ($Co(NH_2)_2$), Dibasic Sodium Phosphate (NaH_2PO_4). All the materials were supplied by Sinopharm Chemical Reagent Co. Ltd.

1.2. Synthesis of Co-Zn LDH@$Co(H_2PO_4)_2$ arrays on NF

The Co-Zn LDH@$Co(H_2PO_4)_2$ arrays were synthesized on Ni foam by a simple hydrothermal method. Typically, a piece of nickel foam with a size of 1.0 ×1.0 cm^2 was pre-treated by HCl solution (3M) for 20 minutes to remove surface impurities, and then washed with deionized water several times. In detail, 0.6 mmol $Zn(NO)_3 \cdot 6H_2O$, 1.2 mmol $Co(NO)_3 \cdot 6H_2O$, 3 mmol $CO(NH_2)_2$ and x mmol NaH_2PO_4 (x=0, 0.18, 0.3, 0.36, 0.42) were dissolved in 60 mL deionized water and magnetically stirred for 15 min. Then, the solution was transferred into a 100 mL Teflon-lined stainless-steel autoclave and a piece of nickel foam was immersed into the reaction solution. The autoclave was heated at 140 ℃ for 8 h and then cooled to room temperature. The NF with the synthesized materials was taken out and washed with ethanol and alcohol several times, respectively. The materials were denoted as Co-Zn LDH (x=0) and Co-Zn LDH@$Co(H_2PO_4)_2$-x (x= 3, 5, 6, 7). The mass loading of the Co-Zn LDH@$Co(H_2PO4)_2$-x on the NF was about 2.1 mg.

1.3. Material Characterizations

The morphology and microstructure of the samples were observed by scanning electron microscopy (SEM, FEI-Quanta 250, USA) and transmission electron microscopy (FE-TEM, GZF20, USA). The elemental analysis of the samples was carried out by scanning electron microscopy (FE-SEM, JSM-7500, Japan) equipped with corresponding energy dispersive x-ray (EDX) element mapping. The elemental composition of the sample was determined by the inductively coupled plasma mass spectrometry(ICP-MS Agilent 725, USA). Surface element analysis of the samples was performed on a PHI 5000 VersaProbe XPS instrument (XPS, Thermo ESCALAB 250XI, USA). The crystal structure of the sample was examined by X-ray diffraction (XRD, Smart Lab, Rigaku, Japan) with Cu-Kα radiation (λ = 1.540598Å, Smart Laboratory).

1.4. Electrochemical Measurements

The electrochemical measurements of the electrodes were performed in 3 M KOH solution on an electrochemical workstation (CHI660E) in a three-electrode testing system. The Co-Zn LDH@$Co(H_2PO_4)_2$ nanoflowers (1×1 cm^2) were used as the working electrode, while platinum plate and Hg/HgO were used as a counter electrode and a reference electrode, respectively. The cyclic voltammetry (CV), electrochemical impedance spectroscopy (EIS) and galvanostatic charge-discharge (GCD) measurements were carried out to evaluate the electrochemical performance of the electrodes. The specific capacity (C g^{-1}) of the electrodes was computed from the GCD curves according to the equation below [1]:

$$Q_s = \frac{I\int_0^{\Delta t} Vdt}{m \times \Delta V_{mean}} = \frac{I\int_0^{\Delta t} Vdt}{m\Delta V} \quad (1)$$

where I, Δt, V, ΔV_{mean}, m, and ΔV are the discharge current (A), discharge time (s), operating potential (V), mean value of operating potential (V), mass (g), and potential window (V) of electroactive materials, respectively.

1.5. Assembly of hybrid supercapacitors

In order to evaluate the practical application of Co-Zn LDH@$Co(H_2PO_4)_2$ electrode, an hybrid double-electrode supercapacitor was assembled using actuated carbon (AC, 11.1mg in 1×1 cm^2) as the negative electrode, the Co-Zn LDH@$Co(H_2PO_4)_2$ (2.1mg in 1×1 cm^2) as the positive electrode and the diaphragm as the diaphragm. The AC was mixed with polyvinylidene fluoride binder (PTFE) and acetylene black in ethanol at a mass ratio of 7:2:1. The NF with synthesized sample (1×1cm^2) was coated with the prepared paste, dried in a vacuum oven at 60℃ for 12 h, and then pressed into a thin film under a pressure of 10 MPa. In order to realize the conservation of charge, the masses of the negative and positive electrodes were balanced by the following equation:

$$\frac{m_+}{m_-} = \frac{C_- V_-}{Q_+} \quad (2)$$

where Q_+, C_-, and V_- are the specific capacity of the positive electrode, the specific capacitance and potential window of AC electrode, respectively.

The following equations can be used to calculate the specific capacity (C g^{-1}), energy density (Wh kg^{-1}) and power density (W kg^{-1}) of the device from the current charge-discharge curves:

$$Q = 2\frac{I\int_0^{\Delta t} V dt}{M\Delta V} \tag{3}$$

$$E = \frac{I\int_0^{\Delta t} V dt}{3.6M} \tag{4}$$

$$P = \frac{3600E}{\Delta t} \tag{5}$$

where I, M, Δt, V and ΔV are the discharge current (A), the total mass of the positive and negative electrode materials (g), discharge time (s), operating voltage (V), and voltage window (V), respectively.

2. Results

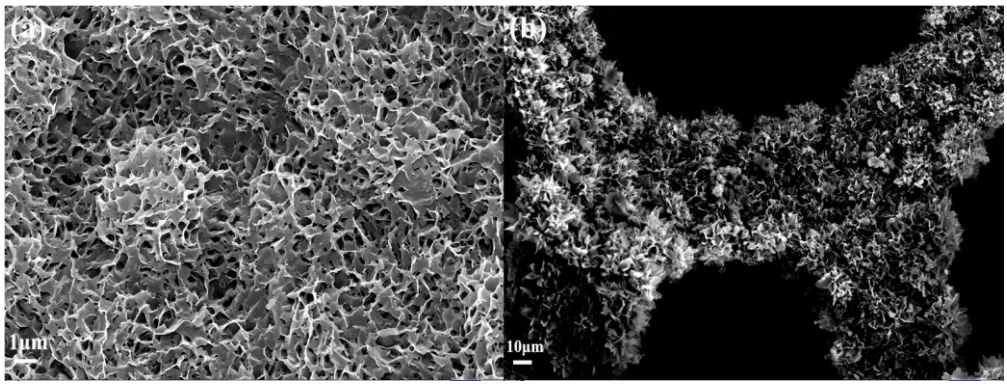

Figure S1. (a) SEM images of Co-Zn LDH; (b) SEM image of Co-Zn LDH@$Co(H_2PO_4)_2$-5.

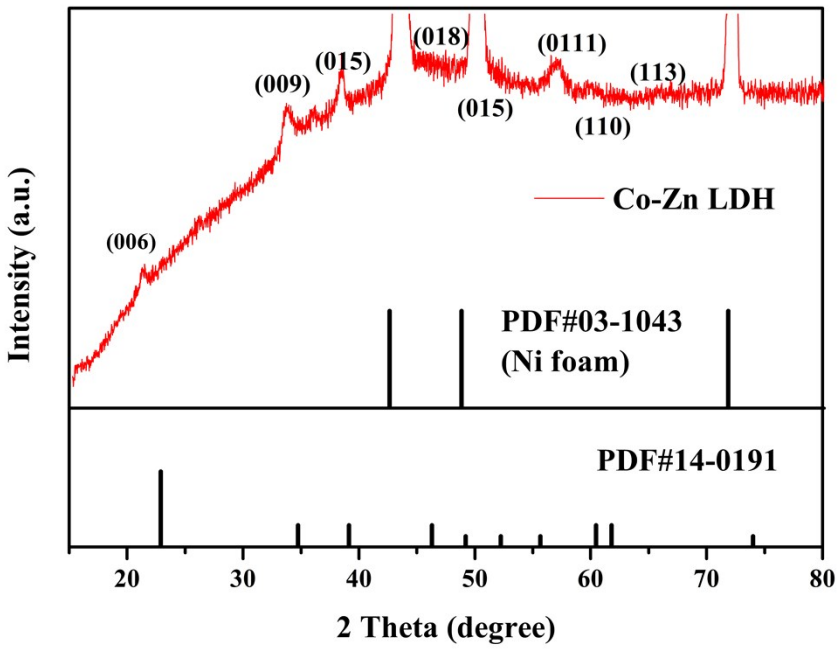

Figure S2. XRD pattern of Co-Zn LDH.

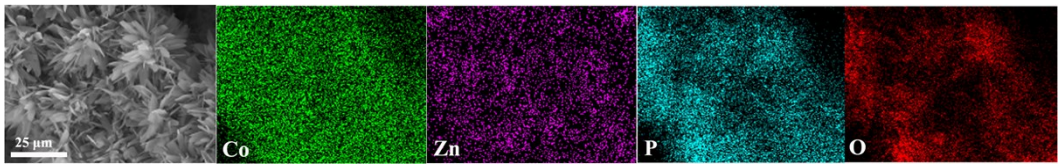

Figure S3. Element mapping of the flower-like structured Co-Zn-LDH@$Co(H_2PO_4)_2$-5.

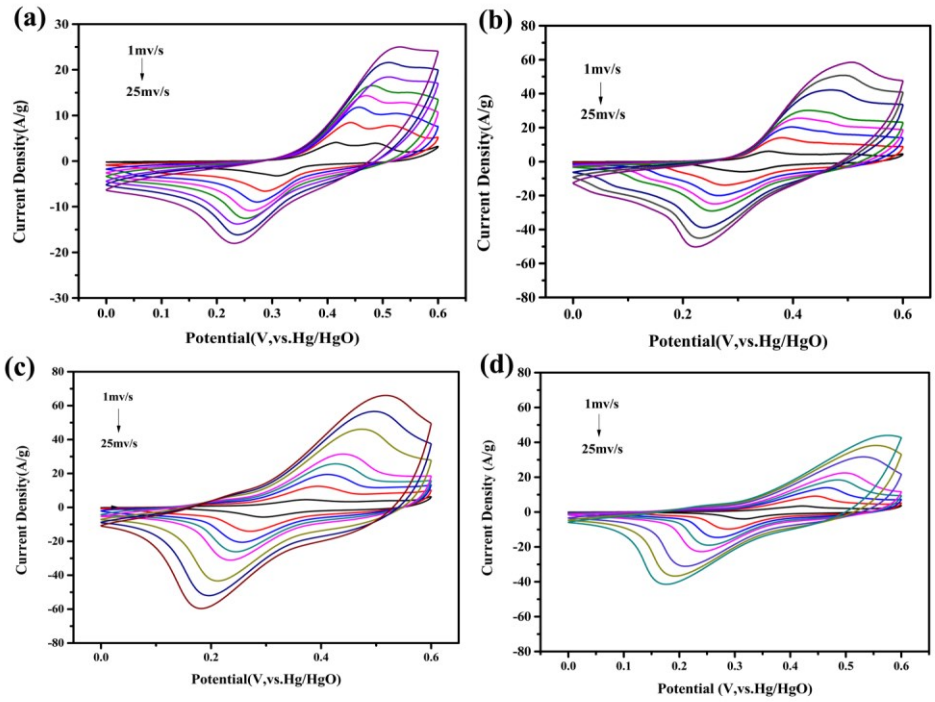

Figure S4. CV curves of the materials at various current densities: (a) Co-Zn LDH; (b) Co-Zn-LDH@$Co(H_2PO_4)_2$-3; (c) Co-Zn-LDH@$Co(H_2PO_4)_2$-6; (d) Co-Zn-LDH@$Co(H_2PO_4)_2$-7.

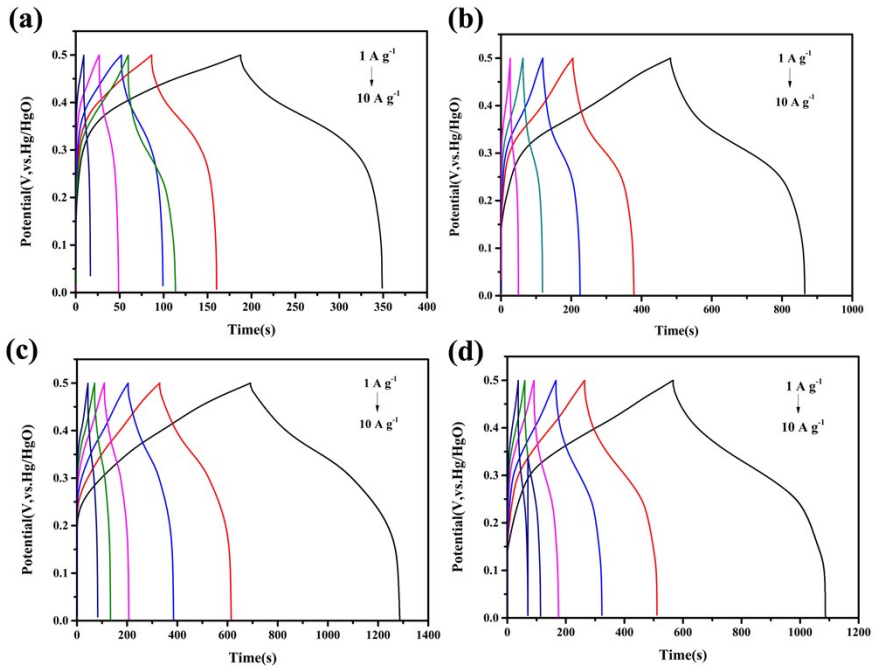

Figure S5. GCD curves of the materials at different current densities: (a) Co-Zn LDH; (b) Co-Zn-LDH@$Co(H_2PO_4)_2$-3; (c) Co-Zn-LDH@$Co(H_2PO_4)_2$-6; (d) Co-Zn-LDH@$Co(H_2PO_4)_2$-7.

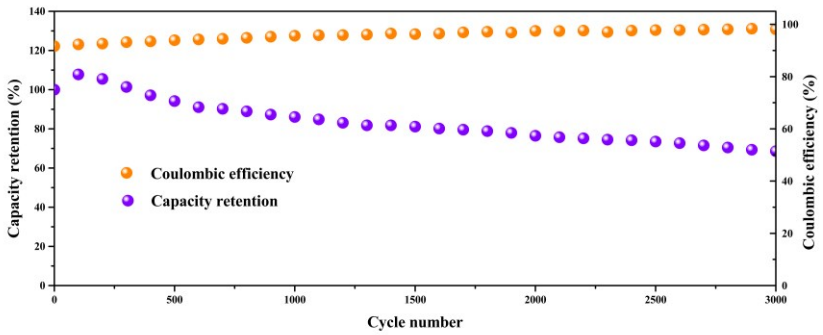

Figure S6. Cycling stability of Co-Zn LDH electrode (2 A g^{-1}).

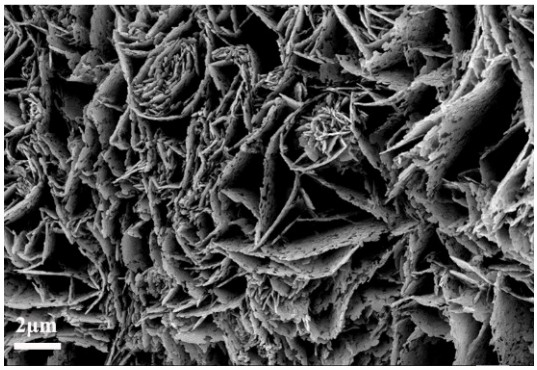

Figure S7. SEM image of the Co-Zn LDH@$Co(H_2PO_4)_2$-5 electrode after cycling test.

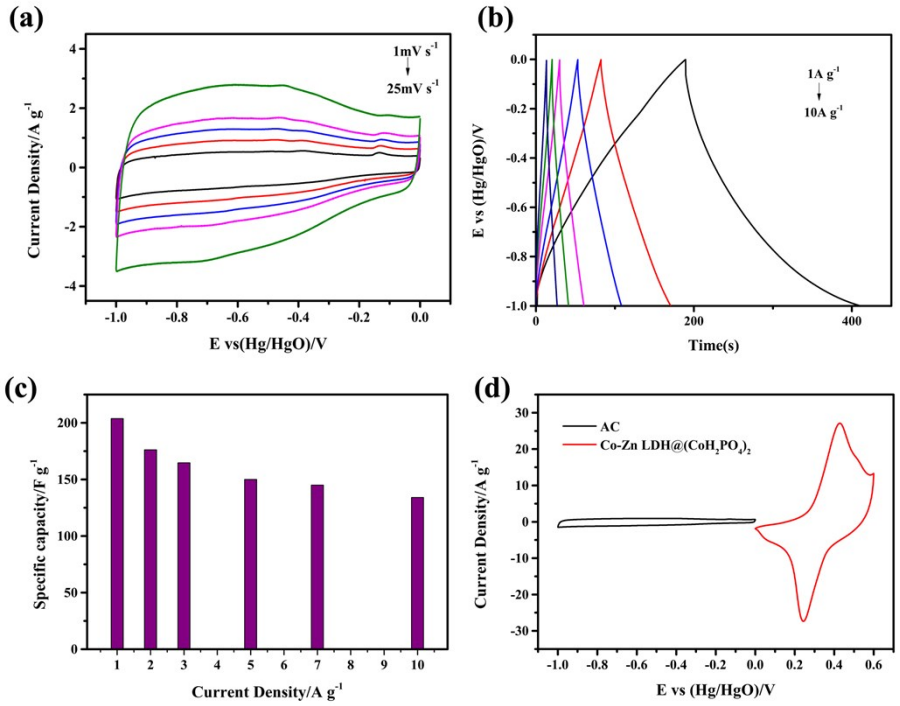

Figure S8. (a) Cyclic curves of AC at different scan rates; (b) Comparison of galvanostatic charge–discharge curves of the AC at different current densities; (c) Specific capacitance of AC at different current densities; (d) Cyclic curves of AC and Co-Zn LDH@$Co(H_2PO_4)_2$-5 at 5 mV s^{-1}.

Table S1. Ion concentration (Wt%) of Zn, Co and P in Co-Zn LDH@$Co(H_2PO_4)_2$-5 as determined through ICP-MS measurements.

	Co	Zn	P
Co-Zn LDH@$Co(H_2PO_4)_2$-5	2.12	4.35	2.02

Table S2. Results of Co-Zn LDH@$Co(H_2PO_4)_2$-5 XPS peak area and element weight ratio.

Name	Peak BE	FWHM eV	Area(P) CPD.eV	Atomic %
O1s C=O/Phosphate	532.4	1.92	58193	26.64
O1s C-O	531.9	1.92	6621.5	3.01
O1sMetal O	531.6	1.92	1497.15	0.685
$P2p_{3/2}$ P-O	132.87	1.4	22704.26	10.39
$P2p_{1/2}$ P-O	133.08	1.4	11596.72	0
$Co2p_{3/2}$ Co^{2+}	781.2	3.24	196943.4	27.03
$Co2p_{1/2}$ Co^{2+}	797.21	3.24	83858.4	0
$Co2p_{3/2}$ Co^{3+}	786.1	6.25	95832.6	13.23
$Co2p_{1/2}$ Co^{3+}	802.85	5.67	53374.5	0
$Zn2p_{3/2}$ Zn^{2+}	1043.8	2.23	182416.28	18.98
$Zn2p_{1/2}$ Zn^{2+}	1020.5	2.23	94486.24	0

Table S3. Results of the weight ratio of Co-Zn LDH and $Co(H_2PO_4)_2$.

	$Co(H_2PO_4)_2$	Co-Zn LDH
O1s C=O/Phosphate	26.64	
O1s C-O		3.01
O1sMetal O	0.685	
$P2p_{3/2}$ P-O	10.39	
$Co2p_{3/2}$ Co^{2+}	27.03	
$Co2p_{3/2}$ Co^{3+}		13.23
$Zn2p_{3/2}$ Zn^{2+}		18.98
Total	64.745	35.22

Table S4. Comparative specific capacitance values of the previously reported transition-metal materials with our Co-Zn LDH@$Co(H_2PO_4)_2$-5 electrode in a three-electrode system.

Materials	Specific capacitance	Current density/scan rate	Ref.
Mxene-NiCo LDH	983.6 F g^{-1}	2 A g^{-1}	2
NiCo-SDBS-LDH	1094 F g^{-1}	5 A g^{-1}	3
ZIF-8-C@NiAl-LDH	1370 F g^{-1}	1 A g^{-1}	4
Ag NW@NiAl LDH	1148 F g^{-1}	1 A g^{-1}	5
CoAl-LDH/FG-12	1222 F g^{-1}	1 A g^{-1}	6
Cactus-like NiCoP/NiCo-OH	1100 F g^{-1}	1 A g^{-1}	7
Ni-Al LDH hollow sphere	1578 F g^{-1}	1 A g^{-1}	8
NiAl-LDH nanoplates	1713 F g^{-1}	1 A g^{-1}	9
KCu_7S_4@NiMn LDH	734 F g^{-1}	1 A g^{-1}	10
$NiCo_2$Al-LDH	1137 F g^{-1}	0.5 A g^{-1}	11
MOF-derived Co-Co LDH	1205 F g^{-1}	1 A g^{-1}	12
Co-Zn LDH@$Co(H_2PO_4)_2$	919 C g^{-1} (1838 F g^{-1})	1 A g^{-1}	This work

Table S5. Results of electrical conductivity measurement performed on Co-Zn LDH and Co-Zn LDH@$Co(H_2PO_4)_2$-5.

Electrode Materials	Resistivity (Ω •cm)	Electrical conductivity (S/cm)
Co-Zn LDH	1.29	775.2
Co-Zn LDH@$Co(H_2PO_4)_2$	0.9	1111

Table S6. Comparative cycle ability of the previously reported electrodes with Co-Zn LDH@$Co(H_2PO_4)_2$-5 electrode.

Electrode material	Capacitance retention	Ref.
NiAl-LDHs/MWCNT/NF	83% (after 1000 cycles)	13
Co-Al LDH/graphene	81% (after 2000 cycles)	14
CoNi-LDHs	77% (after 1000 cycles)	15
NiCoAl-LDH	73.5% (after 3000 cycles)	16
Co-Zn LDH@$Co(H_2PO_4)_2$-5	84.3% (after 3000 cycles)	This work

References

[1] S. Liu, Y. Yin, D. Ni, K. San Hui, K. N. Hui, S. Lee, Energy Storage Materials, 19 (2019) 186-196.

[2] H. Li, F. Musharavati, E. Zalenezhad, X. Chen, K. N. Hui and K. S. Hui, Electrochim. Acta 261 (2018) 178-187.

[3] Y. Lin, X. Xie, X. Wang, B. Zhang, C. Li, H. Wang and L. Wang, Electrochim. Acta 246 (2017) 406-414.

[4] B. Han, G. Cheng, E. Zhang, L. Zhang and X. Wang, Electrochim. Acta 263 (2018) 391-399.

[5] L. Li, K. S. Hui, K. N. Hui, T. Zhang, J. Fu and Y. R. Cho, Chem. Eng. J 348 (2018) 338-349.

[6] W. Peng, H. Li and S. Song, ACS Appl. Mater. Interfaces 9 (2017) 5204-5212.

[7] X. Li, H. Wu, A. M. Elshahawy, L. Wang, S. J. Pennycook, C. Guan and J. Wang, Adv. Funct. Mater, 28 (2018) 1800036.

[8] W. Wang, N. Zhang, Z. Shi, Z. Ye, Q. Gao, M. Zhi and Z. Hong, Chem. Eng. J, 338 (2018) 55-61.

[9] L. Li, K. S. Hui, K. N. Hui, Q. Xia, J. Fu and Y. Cho, J. Alloys Compd 721 (2017) 803-812.

[10] X. L. Guo, J. M. Zhang, W. N. Xu, C. G. Hu, L. Sun and Y. X. Zhang, J. Mater. Chem. A 5 (2017) 20579-20587.

[11] X. Gao, X. Liu, D. Wu, B. Qian, Z. Kou, Z. Pan, Y. Pang, L. Miao, J. Wang, Adv. Funct. Mater 2019, 1903879.

[12] X. Bai, J. Liu, Q. Liu, R. Chen, X. Jing, B. Li and J. Wang, Chem. Eur. J 23 **(**2017) 14839-14847.

[13] B. Wang, G. R. Williams, Z. Chang, M. Jiang, J. Liu, X. Lei and X. Sun, ACS Appl. Mater. Interfaces, 2014, 6, 16304-16311.

[14] L. Zhang, X. Zhang, L. Shen, B. Gao, L. Hao, X. Lu, F. Zhang, B. Ding, C. Yuan, J. Power Sources., 2012, 199, 395-40.

[15] S. B. Kulkarni, A. D. Jagadale, V. S. Kumbhar, R. N. Bulakhe, S. S. Joshi and C. D. Lokhande, Int. J. Hydrogen Energy, 2013, 38, 4046-4053.

[16] P. Li, Y. Jiao, S.Yao, Li.Wang, G.Chen,New J. Chem., 2019,43, 3139-3145.